Antiviral Research 94 (2012) 157–167

Contents lists available at SciVerse ScienceDirect

Antiviral Research

journal homepage: www.elsevier.com/locate/antiviral

Viral genome RNA degradation by sequence-selective, nucleic-acid hydrolyzing antibody inhibits the replication of influenza H9N2 virus without significant cytotoxicity to host cells

Aeyung Kim [a,1], Ja-Yeong Lee [a,1], Sung June Byun [b], Myung-Hee Kwon [c], Yong-Sung Kim [a,*]

[a] Dept. of Molecular Science and Technology, Ajou University, Suwon 443-749, Republic of Korea
[b] Animal Biotechnology Division, National Institute of Animal Science, Rural Development Administration, Suwon 441-706, Republic of Korea
[c] Dept. of Microbiology, Ajou University School of Medicine, Suwon 442-721, Republic of Korea

ARTICLE INFO

Article history:
Received 11 November 2011
Revised 29 February 2012
Accepted 23 March 2012
Available online 30 March 2012

Keywords:
Influenza A virus
H9N2 virus
Genome targeting
Nucleocapsid protein
Catalytic antibody
Protein engineering

ABSTRACT

Influenza A virus infection is a great threat to avian species and humans. Targeting viral proteins by antibody has a limited success due to the antigen drift and shift. Here we present a novel antibody-based antiviral strategy of targeting viral genomic RNA (vRNA) for degradation rather than neutralizing viral proteins. Based on the template of a sequence-nonspecific nucleic acid-hydrolyzing, single domain antibody of the light chain variable domain, 3D8 VL, we generated a synthetic library on the yeast surface by randomizing putative nucleic acid interacting residues. To target nucleocapsid protein (NP)-encoding viral genomic RNA (NP-vRNA) of H9N2 influenza virus, the library was screened against a 18-nucleotide single stranded nucleic acid substrate, dubbed asNP_{18}, the sequence of which is unique to the NP-vRNA. We isolated a 3D8 VL variant, NP25, that had ~15-fold higher affinity (~54 nM) and ~3-fold greater selective hydrolyzing activity for the target substrate than for off targets. In contrast to 3D8 VL WT, asNP_{18}-selective NP25 constitutively expressed in the cytosol of human lung carcinoma A549 cells does not exhibit any significant cytotoxicity and selectively degrades a reporter mRNA carrying the target asNP_{18} sequence in the stable cell lines. NP25 more potently inhibits the replication of H9N2 influenza virus than 3D8 VL WT in the stable cell lines. NP25 more selectively reduces the amount of the targeted NP-vRNA than 3D8 VL WT from the early stage of virus infection in the stable cell lines, without noticeable harmful effects on the endogenous mRNA, suggesting that NP25 indeed more specifically recognizes to hydrolyze the target NP-vRNA of H9N2 virus than off-targets. Our results provide a new strategy of targeting viral genomic RNA for degradation by antibody for the prevention of influenza virus infection in humans and animals.

1. Introduction

Influenza A viruses, causing recurrent epidemics and global pandemics in humans and/or some animal species, are of great concern in human health and agricultural economy (Subbarao and Joseph, 2007). The virus has a segmented genome of eight single stranded (ss) (−)-sense RNA molecules that encode 11 viral proteins, including the two surface glycoproteins, hemagglutinin (HA) and neuraminidase (NA), an ion channel protein (M2), and a nucleocapsid protein (NP) which encapsidates the viral genomic RNAs (vRNAs) (Medina and Garcia-Sastre, 2011; Subbarao and Joseph, 2007). On the basis of the antigenicity of their HA and NA molecules, influenza A viruses are classified into 16 HA subtypes (H1–H16) and 9 NA subtypes (N1–N9) (Medina and Garcia-Sastre, 2011; Subbarao and Joseph, 2007).

Current strategies for the prevention and control of influenza virus infections are mainly two: vaccines and antiviral drugs (Kao et al., 2010; Subbarao and Joseph, 2007). The action of mechanisms of antiviral drugs, such as small molecules and monoclonal antibodies (mAbs) are blocking viral proteins involved in the entrance, maturation or departure of the targeted virus into, within and from host cells (Subbarao and Joseph, 2007). Despite of intensive efforts, however, existing vaccines and antiviral drugs against viral proteins are limited in part because of the properties of antigenic shift and drift (Medina and Garcia-Sastre, 2011). Particularly targeting viral proteins by mAb has a limited success due to the difficulty in finding proper epitopes for neutralization (Medina and Garcia-Sastre, 2011). RNA interference, in which double stranded (ds) RNA in length of 21–23 bps, so called small inferring

* Corresponding author. Address: Dept. of Molecular Science and Technology, Ajou University, San 5, Woncheon-dong, Yeongtong-gu, Suwon 443-749, Republic of Korea. Tel.: +82 31 219 2662; fax: +82 31 219 2394.
E-mail address: kimys@ajou.ac.kr (Y.-S. Kim).
[1] The two authors contributed equally to this work.

0166-3542/$ - see front matter © 2012 Elsevier B.V. All rights reserved.
http://dx.doi.org/10.1016/j.antiviral.2012.03.007

RNA (siRNA), directs sequence-specific degradation of messenger RNA (mRNA). Thus siRNAs targeting viral mRNAs have been extensively explored as an effective antiviral strategy for its specific silencing of viral gene expression in mammalian cells (Barik, 2010), including NP and M2 genes of influenza A viruses (Ge et al., 2003; Sui et al., 2009; Zhou et al., 2007, 2008). However, siRNAs have never been exploited to directly target viral vRNAs.

Another approach to antiviral therapy by degrading viral RNAs is the use of ribonucleases (RNases). For examples, the human RNase ISG20 and amphibian Onconase from a frog of *Rana pipiens* substantially suppressed the infection and accumulation of vesicular stomatitis and influenza viruses in HeLa cells (Espert et al., 2003) and human immunodeficiency type I virus (HIV-1) in a chronically HIV-1-infected human cells (Saxena et al., 1996, 2002), respectively. Very recently, we have also shown that 3D8 single-chain variable fragment antibody (scFv) with the DNA/RNA-hydrolyzing catalytic activity without sequence specificity also reduced the replication of classical swine fever virus (CSFV) in a porcine kidney cells (Jun et al., 2010). However, Onconase and 3D8 scFv, which lack the sequence specificity of RNA, have shown undesirable cellular cytotoxicity to the host cells most likely due to sequence-nonspecific hydrolysis of cellular RNAs (Jang et al., 2009; Jun et al., 2010; Smith et al., 1999). Thus we hypothesized that engineering of the antiviral nucleases to have sequence specificity against viral RNAs can overcome the undesirable cytotoxicity, while maintaining the antiviral activity.

Previously we have shown that the single domain antibody of light chain variable domain, 3D8 VL, possesses DNA/RNA-hydrolyzing activity, but does not have particular sequence specificity (Kim et al., 2006, 2009). We recently engineered 3D8 VL to have sequence specificity against given 18-nucleotide (nt) ssDNA substrates by randomizing residues putatively interacting with nucleic acids while preserving the hydrolyzing activity (Lee et al., 2010b). The engineered 3D8 VL variants selectively decreased the amount of target sequence-carrying mRNAs in the cytosolic environment, inducing the target gene-selective gene silencing (Lee et al., 2010b).

To achieve the inhibition of influenza viral replication, we here describe a proof-of-concept of targeting viral genome vRNA for degradation by antibody with the sequence-specific nuclease catalytic activity rather than the viral proteins or mRNAs. As a model system, we target the NP-encoding vRNA (NP-vRNA) of the low pathogenic avian influenza H9N2 virus (A/Chicken/Korea/MS96/96) (Kwon et al., 2010). H9N2 viruses are the most abundant influenza virus isolated from live-poultry in Korea (Choi et al., 2005). Influenza NP is the most abundantly expressed protein during the course of infection and essential for viral replication, serving as an ideal target for antiviral therapy (Kao et al., 2010). To target NP gene at the viral genome vRNA level, we engineered the sequence non-specific DNA/RNA-hydrolyzing 3D8 VL into a target sequence-selective hydrolyzing variant, dubbed NP25, against an 18-nt ssDNA with a sequence derived from the H9N2 NP-vRNA. The constitutive expression of NP25 in the cytosol of human lung carcinoma A549 cells potently protected the stable cell lines from the replication of H9N2 virus by selectively decreasing the amount of the targeted NP-vRNA without significant cytotoxicity to the host cells. Our results provide a basis for the development of antiviral antibody targeting influenza viral genome for degradation.

2. Materials and methods

2.1. Cell lines and reagents

Human lung adenocarcinoma epithelial cell line, A549 cells were purchased from American Type Culture Collection (ATCC, Manassas, VA) and maintained in Dulbecco's Modified Eagle Medium (DMEM; Welgene, Korea) supplemented with 10% (v/v) heat-inactivated fetal bovine serum (FBS; GIBCO/Invitrogen, Carlsbad, CA) and 100 units/ml of penicillin/100 μg/ml of streptomycin (Welgene) at 37 °C in a humidified 5% CO_2 incubator. All oligonucleotides were synthesized from Bioneer Co. (Korea), unless otherwise specified. Target 18-nt ssDNA substrate, asNP_{18} (5′-GGU CUG GCA CUU UCC AUC-3′), and off-target 18-nt ssDNA, N_{18} (5′-NNN NNN NNN NNN NNN NNN-3′) (N = A/T/G/C), were synthesized with or without 5′-biotinylation (Lee et al., 2010b). All other reagents were analytical grade. Rabbit anti-3D8 polyclonal antibodies, which also bind to 3D8 VL WT and its variant NP25, were produced by immunization in our laboratory (Lee et al., 2010b). Streptavidin conjugated R-phycoerythrin (SA-PE) from Molecular Probes (CA, USA), rabbit anti-$p21^{Cip1}$ antibody from Cell Signaling Technology (Danvers, MA), mouse anti-c-myc mAb from Ig Therapy (Chunchun, Korea), rabbit FITC-conjugated anti-mouse IgG and goat TRITC-conjugated anti-rabbit IgG from Thermo Scientific (Rockford, IL), and rabbit anti-cyclin D1, rabbit anti-β-actin, mouse anti-NP mAb, goat FITC-labeled anti-rabbit IgG, and rabbit anti-GFP IgG from Santa Cruz Biotechnology (Santa Cruz, CA) were used.

2.2. 3D8 VL library construction and screening

3D8 VL with His94Ala mutation (hereafter designated as 3D8 VL WT), which possessed higher nuclease activity than the original 3D8 VL with His94 (Kim et al., 2006), was used as a template for the library construction. We designed a 3D8 VL library by randomizing only the surface exposed residues in C-strand (Ala34, Tyr36, and Gln38), C′-strand (Pro44 and Leu46), and F-strand (Ala84, Val85, and Tyr87), and G-strand (Lys103 and Glu105) with a degenerate codon of NNB (N = A/T/G/C, B = C/G/T) (Supplementary Fig. S1). The 3D8 VL library was generated by serial overlapping PCRs to reconstitute full-size products using five partially overlapping oligonucleotides and two flanking oligonucleotides, as described previously (Lee et al., 2010b). The amplified 3D8 VL gene library (10 μg) and linearized yeast surface display plasmid pCTCON (1 μg) with *Nhe*I/*Bam*HI sites were cotransformed ten times into *Saccharomyces cerevisiae* EBY100 strain by homologous recombination technique using a Bio-Rad Gene Pulser electroporation apparatus (Lee et al., 2010a). Library size determined by plating serial 10-fold dilutions of the transformed cell on the selective agar plates was about 1.1×10^8. Sequencing of randomly chosen 25 clones from the unscreened library exhibited mutations only at the targeted regions. The cell-surface expression and 18-nt ssDNA binding levels of 3D8 VL library were determined using flow cytometry by indirect double immunofluorescence labeling of a C-terminal c-myc tag (anti-c-myc mAb/FITC-labeled anti-mouse mAb) and 5′-biotinylated ssDNA substrates (each biotinylated substrate/SA-PE), respectively (Lee et al., 2010a).

2.3. Screening of 3D8 VL library against the target ssDNA substrate

For the library screening against the target asNP_{18} ssDNA substrate, 2 rounds of MACS (magnetic-activated cell sorting) and then subsequent 4 rounds of FACS (fluorescence-activated cell sorting) were sequentially carried out using the biotinlyated-asNP_{18} substrate following the protocol described previously (Lee et al., 2010b). Briefly, yeast cells were labeled with 5 and 1 μM of biotinylated-asNP_{18} in TBSE buffer (25 mM Tris–HCl, pH 7.4, plus 137 mM NaCl, 2.7 mM KCl, 0.5% BSA and 2.5 mM EDTA) in the first and second round of MACS, respectively. In the FACS screening, TBSF buffer (TBSE plus additional 150 mM NaCl) was used during the substrate labeling. Further, sorting stringency was increased by decreasing the asNP_{18} substrate concentration and increasing off-target ssDNA N_{18} competitor concentration: 1 μM asNP_{18} and 1 μM N_{18} (1:1 competition) in round 1, 1 μM asNP_{18} and

50 μM N_{18} (1:50 competition) in round 2, 0.5 μM $asNP_{18}$ and 50 μM N_{18} (1:100 competition) in round 3, and 0.2 μM $asNP_{18}$ and 50 μM N_{18} (1:250 competition) in round 4. Typically, the top 0.5–1% of target-binding cells was sorted using FACSAria II (BD Bioscience). The finally sorted yeast cells were plated on the selective medium and individual clones were further characterized.

2.4. Protein expression and purification

3D8 VL WT subcloned into a bacterial secretion plasmid pIg20 was expressed in *Escherichia coli* strain BL21 (DE3) pLysE (Novagen) and purified from the supernatant of bacterial culture using the IgG-Sepharose™ column (GE Healthcare), as described previously (Kim et al., 2006; Lee et al., 2010b). Isolated 3D8 VL variants were subcloned using *Xba*I and *Bam*HI into pET32b vector (Novagen), resulting in pET32b-VL variants, which has N-terminal 6× His tag, C-terminal Thioredoxin A (TrxA), and enterokinase cleavage sequence between TrxA and VL variants (Supplementary Fig. S2A). The plasmid pET32b-VL was transformed into *E. coli* BL21 (DE3). After the transformants were grown at 30 °C to an OD_{600} of ~0.8 in 300 ml of Luria–Bertani medium, protein expression was induced by addition of 0.5 mM isopropyl-β-D-1-thiogalactoside. After 4 h induction at 20 °C, cells were harvested by centrifugation at 8000*g* for 20 min at 4 °C, resuspended in a 10 ml lysis buffer (50 mM phosphate at pH 8.0, 300 mM NaCl, 5 mM imidazole, 1 mM DTT, 10% glycerol, 1 mM PMSF protease inhibitor) and disrupted by sonication on ice-cold distilled water with 10 s pulses at high intensity for 15 min. Proteins were purified from the cell lysates using anti-6× His Talon resin (Clontech Lab) as described previously (Lee et al., 2010a). Protein concentrations were determined using extinction coefficients calculated from the respective amino acid sequence and also confirmed by Bradford assay (Bio-Rad) (Lee et al., 2010b).

2.5. Sequence-specific 18-nt ssDNA hydrolyzing assay and other biochemical analyses of proteins

Sequence-specific 18-nt ssDNA hydrolyzing kinetic assays of 3D8 VL WT and its variants were carried out by FRET-based cleavage assay as described previously (Lee et al., 2010b). The 18-nt ssDNA $asNP_{18}$ and N_{18} substrates, which were double-labeled with a 6-carboxyfluoroscein (FAM™) at the 5′-terminus and a black hole quencher (BHQ®-1) at the 3′-terminus (Integrated DNA Technologies), were used. The apparent enzymatic kinetic parameters, K_m and V_{max}, were determined by fitting the initial rate constants (V) versus substrate concentrations (S) into the Michaelis–Menten equation ($V = (V_{max}[S])/(K_m + [S])$) and Lineweaver–Burk equation using Sigmaplot 2002 software (SPSS Inc.) (Kim et al., 2009; Lee et al., 2010b). Biochemical analyses of 3D8 VLs, such as DNA-hydrolyzing assays on agarose gels and surface plasmon resonance (SPR), were performed as described previously (Kim et al., 2006, 2009; Lee et al., 2010b).

2.6. Establishment of stable A549 cell lines expressing 3D8 VL WT or NP25

The coding sequences of 3D8 VL WT and its variant NP25 were PCR amplified with a Kozak-consensus sequence upstream of the start codon and a C-terminal c-myc tag and then subcloned into pcDNA3.1(+) (Invitrogen Inc.) with *Nhe*I and *Bam*HI sites, resulting in pcDNA3.1-3D8 VL WT or pcDNA3.1-NP25 (Lee et al., 2010b). For the expression of 3D8 VL WT or NP25, A549 cells grown ~50% confluency (~5×10^5 cells in 60-mm dishes) were transfected with plasmid of pcDNA3.1-VL WT or pcDNA3.1-NP25 (each 3 μg) using WelFect-EX™ PLUS transfection reagent kit (Welgene, Korea) according to the manufacturer's instruction. After 24 h of culture in 10% FBS/DMEM, cells were plated by limiting dilution in media containing 1 mg/ml G418 (Sigma) for 10–14 days. Wells containing single G418-resistant clones were expanded and screened by fluorescence microscopy for 3D8 VL WT or NP25 expression and by Western blotting for myc expression. Then, transfected cells constitutively expressing 3D8 VL WT (WT-1 and WT-2 cells) and NP25 (NP25-1 and NP25-2 cells) at a similar level were selected for this study. Mock cells transfected with the empty plasmid of pcDNA3.1(+) (3 μg) were also established by G418 selection for 10–14 days.

2.7. Cell proliferation assay

To examine effects of 3D8 VL WT and NP25 expression on the cell growth rate, cells were seeded on a 6-well culture plate at a density of 1×10^5 cells/well and then viable cells were counted on a hemocytometer by staining cells with 0.4% trypan blue/PBS solution every 24 h for 3 days. The population doubling time was calculated using *Doubling Time Software v1.0.10* (http://www.doubling-time.com).

2.8. Analysis of EGFP expression in A549 cells constitutively expressing 3D8 VL WT or NP25

For the cytosolic expression of enhanced green fluorescent protein (EGFP), pEGFP-N1 (Clontech, the GFP carries two mutations of Phe64Leu and Ser65Thr) was used without any modification (Lee et al., 2010b). To construct EGFP reporter plasmid, the target sequence of $asNP_{18}$ or off-target sequence of G_{18} with contiguous 18 Guanine nucleobases was placed between the ATG start codon and EGFP coding sequence in the pEGFP-N1 plasmid, resulting in $pasNP_{18}$-EGFP and pG_{18}-EGFP, respectively (Lee et al., 2010b). The established mock, WT-1/-2, and NP25-1/-2 cells were transfected for 4 h using WelFect- EX™ PLUS transfection reagent kit with the plasmid of pEGFP-N1, $pasNP_{18}$-EGFP or pG_{18}-EGFP and then incubated for 24 h prior to monitoring of EGFP expression by semi-quantitative RT-PCR, Western blotting, confocal fluorescence microscopy, and flow cytometry, as described previously (Lee et al., 2010b).

2.9. Influenza H9N2 virus infection

A low pathogenic avian influenza H9N2 (A/Chicken/Korea/MS96/96) virus (Kwon et al., 2010), which caused disease in chickens in Korea in 1996, were kindly provided from the National Veterinary Research and Quarantine Service (NVRQS), Korea. The H9N2 virus was propagated in the pathogen-free fertilized eggs by viral injection into allantoic cavity (Kwon et al., 2010). The low pathogenicity of H9N2 virus did not form plaque in A549 cells (Supplementary Fig. S3) (Kwon et al., 2010; Wan et al., 2008). The titer of virus stock was determined in A549 cells by the 50% tissue culture infective dose ($TCID_{50}$), the virus dose that is able to infect 50% of the cell cultures, following the standard protocol (Daelemans et al., 2011). Briefly, A549 cells (1×10^4 cells/well in 96-well plates) were challenged with serial 5-fold dilutions of virus sample and then incubated at 37 °C under 5% CO_2 for 3 days. Then, the cells were examined microscopically for H9N2-induced cytopathic effect to determine the $TCID_{50}$. Then the plaque-forming unit (PFU) is predicted by multiplying the $TCID_{50}$ by 0.7 (Daelemans et al., 2011). The titers of the viral stock were usually 1–2 × 10^4 $TCID_{50}$/ml (0.7–1.4 × 10^4 PFU/ml).

For the H9N2 virus infection into cells, culture medium was removed, and then H9N2 virus in infection medium (PBS, 0.3% BSA, 1 μM $MgCl_2$, 1 μM $CaCl_2$, 100 units/ml penicillin, 100 μg/ml streptomycin, and 4 μg/ml trypsin) was added into cells at the indicated multiplicity of infection (m.o.i.). After incubation for 1 h at 25 °C,

fresh infection medium (DMEM, 0.3% BSA, and 4 μg/ml trypsin) was added, and the cells were cultured for the indicated periods at 37 °C under 5% CO_2.

2.10. Hemaggutination (HA) assay

To determine virus titer in the culture supernatants of H9N2-infected cells, HA assay was carried out for the serially diluted culture supernatants in U-bottom 96-well plates according to the previous method (Kwon et al., 2010). Cells seeded on 6-well culture plates (5×10^4 cells/well) were infected with H9N2 virus at the indicated m.o.i. for 1 h at 25 °C. After washing three times with PBSB (PBS plus 0.3% BSA) buffer, cells were incubated in the infection medium (DMEM, 0.3% BSA, and 4 μg/ml trypsin). At the indicated hpi (hour of post-infection), culture supernatants were collected by centrifugation at 12,000 rpm for 5 min to remove cell debris, and then stored at -80 °C before use. Serial 2-fold dilutions of culture supernatant (in PBS, 25 μl) were mixed with an equal volume of a 1% suspension (v/v, 0.1 M PBS) of chicken erythrocytes, and then incubated plates on ice for 1 h. Wells containing an adherent, homogenous layer of erythrocytes were scored as positive, while wells appeared as dots in the center of round U-bottomed plates as negative.

2.11. Immunofluorescence microscopy

For the detection of 3D8 VL WT or NP25 expressed in the stable A549 cell lines, immunofluorescence microscopic analyses were performed. Briefly, cells seeded on the glass coverslips at a density of 5×10^4 cells/well in 24-well culture plate were fixed with 2% paraformaldehyde (PFA) in PBS for 10 min at 25 °C, and then permeabilized with PERM-Buffer (0.1% saponin, 0.1% sodium azide, 1% BSA in PBS) for 10 min at 25 °C. After blocking with 2% BSA in PBS for 1 h at 25 °C, cells were stained with rabbit anti-3D8 polyclonal antibodies (diluted 1:500 in 2% BSA in PBS) for 2 h at 25 °C, followed by TRITC-conjugated anti-rabbit IgG (1:500) for 1 h at 25 °C. Coverslips were mounted on glass slides with VECTASHIED (mounting medium with DAPI, Vector Laboratories, Burlingame, CA) and observed with fluorescence microscope (Axio Imager AI, Carl Zeiss Microimaging GmbH, Germany). The NP level in the H9N2 virus-infected cells was also examined under fluorescence microscope after staining with mouse anti-NP Ab (1:100), followed by FITC-conjugated anti-mouse IgG (1:500).

2.12. Western blotting

Whole cell lysates were extracted using M-PER Mammalian Protein Extraction Reagent (Thermo Scientific), and protein concentrations were determined using Bicinchoninic Acid (BCA) Kit (Sigma). After immunoblotting, proteins were visualized using a PowerOpti-ECL Western blotting Detection reagent (Animal Genetics, Inc. Korea) and an ImageQuant LAS 4000 mini (GE Healthcare, Piscataway, NJ) (Lee et al., 2010b; Sung et al., 2010). Equal amount of proteins was analyzed by Western blots using β-actin as a loading control. Band densities were quantified using ImageJ software (National institutes of Health, USA).

2.13. RNA extraction and RT-PCR

After infection of cells with H9N2 virus at the indicated m.o.i. for 1 and/or 3 h, total RNA was extracted using PureHelix™ RNA Extraction solution (NanoHelix Co., Daejeon, Korea) following the manufacturer's instructions and reverse-transcription (RT) was carried out using HelixCript™ 1'st strand cDNA synthesis kit (NanoHelix Co.) in a 20 μl reaction mixture, containing 3 μg of total RNA. Quantitative real-time PCR was performed using gene-specific primers by using Chromo4™ Real-Time Detector (BioRad) with RealHelix™ qPCR kit (NanoHelix Co.), and the levels of PCR products were analyzed with Opticon Monitor Software. A threshold was set above the baseline and a threshold cycle value (C*t*) was defined as the cycle number at which the fluorescence passes the fixed threshold. For each viral RNA, the duplicate C*t* values were averaged and normalized to those of α-tubulin mRNA and then represented as fold differences compared with the normalized C*t* values of mock cells. cDNA aliquots were also analyzed by semi-quantitative PCR, and the PCR products were electrophoresed on 1% agarose gels and stained with ethidium bromide. Band intensity was quantitatively analyzed using ImageJ software for each gene. Primer sequences for RT-PCR and real-time PCR analysis are shown in Supplementary Table S1.

2.14. Statistical analysis

Data are reported as mean ± SEM of two or three independent experiments carried out in triplicate. Statistical significance was analyzed by a two-tailed Student's *t*-test on Sigma Plot 8.0 software (SPSS Inc.) and a *P* value of less than 0.05 was considered significant.

3. Results

3.1. Target sequence selection of NP-vRNA from H9N2 influenza virus

A low pathogenic avian influenza H9N2 virus (A/Chicken/Korea/MS96/96) (Kwon et al., 2010) was used as a model virus in this study. To target the NP-vRNA located in segment 5 of H9N2 viral genome (Subbarao and Joseph, 2007), a 18-nt sequence corresponding to positions 150–167 of the antisense (−) NP-vRNA (NCBI Accession No. AF203787) was chosen as a target substrate because the sequence does not share identity more than 60% with any other human mRNAs. Further sequence alignment of NP-vRNA of H9N2 virus against other influenza viral NP-vRNAs in the influenza sequence database (www.flu.lanl.gov) revealed that the regions are extremely conserved (no more than one mismatch in 18-nt sequence) in different virus subtypes and strains, including high pathogenic viruses of H1N1 (A/PuertoRico/8/34) and H5N1 (A/chicken/Hubei/327/2004). The complimentary sequence of the 18-nt sequence has been validated as an effective siRNA target region for the sense (+) NP-mRNA of H9N2, H5N1 and H1N1 viruses (Zhou et al., 2007). We synthesized the substrate as 18-nt ssDNA, dubbed asNP_{18}, rather than ssRNA due to the higher nucleolytic stability, but used uracil base instead of thymine base to retain the primary structure.

3.2. 3D8 VL library construction and screening the library against the target asNP_{18} substrate

We constructed a yeast surface-displayed 3D8 VL library with a diversity about 1.1×10^8 by randomizing 10 putative nucleic acid-interacting residues located in one of two β-sheets with a degenerate codon of NNB (Supplementary Fig. S1A), while preserving the catalytic residues located in the upper part of the mutated β-sheet (Lee et al., 2010b; Park et al., 2008). Using the 5′-biotinylated 18-nt ssDNA asNP_{18} substrate, we carried out two rounds of MACS followed by four rounds of FACS to isolate the target-specific recognizing 3D8 VL variants. During MACS and FACS screenings, the substrate labeling buffer contained 2 mM EDTA to protect ssDNA substrates from hydrolyzing by displayed 3D8 VL variants and 300 mM NaCl to counterselect against non-specific binders that interacts with DNA phosphate backbone through electrostatic interactions. To ensure that isolated 3D8 VL variants will bind preferentially to the target sequence, we also added non-biotinylated

off-target competitor N_{18} (N = A/T/G/C) in high molar ratios to the target substrate (from 1:1 to 250:1) in the substrate labeling step during FACS. Thirty clones were sequenced after the final round of FACS, and five 3D8 VL variants with unique mutated sequences at the targeted residues were obtained (Supplementary Fig. S1B). The isolated 3D8 VL variants in the yeast-surface displayed form showed more than 2-fold higher binding level with the target asNP_{18} than off-target N_{18} (Supplementary Fig. S1C), compared with the WT that exhibited indistinguishable binding levels between asNP_{18} and N_{18}.

3.3. Selected NP25 variant against asNP_{18} substrate shows preferential binding and hydrolyzing activities for the target substrate

To further characterize in soluble forms, the isolated variants were expressed in *E. coli*. While 3D8 VL WT were expressed solubly by the periplasmic targeting (Kim et al., 2006; Lee et al., 2010b), all of the isolated variants were expressed dominantly in insoluble form of inclusion body, regardless of cytosolic or periplasmic expression. Thus each variant was prepared in soluble form by cytoplasmic expression after its C-terminal fusion to TrxA (Supplementary Figs. S2A and S2B).

DNA hydrolyzing activity analyses of the purified variants by agarose gel electrophoresis using the supercoiled plasmid of pUC19 as a substrate demonstrated that they maintained the Mg^{2+}-dependent DNA-hydrolyzing catalytic activity, like the WT (Supplementary Fig. S2C) (Kim et al., 2006; Lee et al., 2010b). The target sequence-selective hydrolyzing activity of the isolated variants was determined by FRET (fluorescence resonance energy transfer)-based cleavage assay using the target asNP_{18} and off-target N_{18} ssDNAs, which were double-labeled with a fluorophore (FAM) at 5′-terminus and its quencher (BHQ®-1) at 3′-terminus (Jang et al., 2009; Lee et al., 2010b). The substrate hydrolyzing activity can be monitored by following the fluorescence intensity increase caused by the 6-FAM release from its quencher BHQ®-1 due to the hydrolysis (Jang et al., 2009; Lee et al., 2010b). Among the primarily isolated five variants, NP25 showed the most target sequence-selective hydrolyzing activity (Supplementary Fig. S4). Thus we chose NP25 for further studies.

We compared the binding specificity and affinity between 3D8 VL WT and NP25 for the target asNP_{18} and off-target N_{18} ssDNA substrates using SPR technique (Lee et al., 2010b). While 3D8 VL WT exhibited indistinguishable binding affinities ($K_D \approx 5$ μM) for both asNP_{18} and N_{18} (Kim et al., 2006, 2009; Lee et al., 2010b), NP25 showed ~15-fold tighter binding to the target asNP_{18} ($K_D \approx 54$ nM) than to the off-target N_{18} ($K_D \approx 822$ nM) (Fig. 1A and Table 1). Next, the target sequence-selective hydrolyzing activity of NP25 was measured by FRET assay using various concentrations of substrates, in comparison with 3D8 VL WT (Fig. 1B). NP25 hydrolyzed ~3-fold more efficiently the target asNP_{18} substrate ($k_{cat}/K_m \approx 4.8 \times 10^{-6}$ $nM^{-1}s^{-1}$) than the off-target N_{18} ($k_{cat}/K_m \approx 1.4 \times 10^{-6}$ $nM^{-1}s^{-1}$) due to their improved substrate affinity (K_m) and catalytic rates (k_{cat}), whereas 3D8 VL WT exhibited similar hydrolyzing efficiencies ($k_{cat}/K_m \approx 2.6–3.5 \times 10^{-6}$ nM^{-1} s^{-1}) for the two substrates (Table 2). Taken together, these results demonstrated that, compared with 3D8 VL WT, NP25 isolated against asNP_{18} preferentially recognizes and degrades the target substrate over the off-target substrate, designating NP25 as an asNP_{18}-selective hydrolyzing variant.

3.4. Constitutive expression of NP25 does not show significant cytotoxicity mediated by its WT in the stable A549 cell lines

To evaluate the antiviral activity of asNP_{18}-selective NP25 in the cellular environment, we first established A549 cell lines constitutively expressing NP25 or 3D8 VL WT as a control. Mock cells transfected by the empty plasmid with no 3D8 VL gene were also established (Fig. 2A). Among more than 20 clones that were selected as positive for the expression of NP25 or 3D8 VL WT, we selected two representative clones for NP25 (dubbed NP25-1 and NP25-2 cells) and WT (dubbed WT-1 and WT-2 cells), respectively, which are all expressing very similar levels of the proteins based on confocal fluorescence microscopy (Fig. 2A) and Western blotting (Fig. 2B). 3D8 VL WT and NP25 are predominantly localized in the cytosol of cells with little accumulation in the nucleus (Fig. 2A).

In our previous studies we found that 3D8 antibody either in scFv or VL format caused some cytotoxicity in the host cells, which was probably due to the sequence non-specific cellular RNA hydrolysis (Jang et al., 2009; Jun et al., 2010; Lee et al., 2010b). When we examined effects of the constitutive expression of 3D8 VL WT and NP25 on the cell growth rates in the established cell lines, WT-1/-2 cells expressing 3D8 VL WT showed ~1.2-fold slower proliferation rates (population doubling time of ~25.2 h) than the plasmid-only transfected mock cells (population doubling time of ~21.3 h) (Fig. 2C), suggesting that the cytosolic expression of 3D8 VL WT is somewhat cytotoxic to the host cells. However, NP25-1/-2 cells exhibited very similar cell growth rates (population doubling time of ~20.8 h) to those of the mock cells (Fig. 2C). A previous study showed that microinjection of RNase proteins into human NIH/3T3 cells retarded the cell growth rate by G_0/G_1 cell cycle arrest (Smith et al., 1999). To determine whether 3D8 VL WT-mediated growth inhibition was also mediated by G_0/G_1 cell cycle arrest, we monitored the expression levels of the representative cell cycle-associated proteins, $p21^{Cip1}$ and cyclin D1 (Sherr and Roberts, 1995). Compared with the mock cells, WT-1/-2 cells, but not NP25-1/-2 cells, showed upregulation of $p21^{Cip1}$ and downregulation of cyclin D1 (Fig. 2D), indicative of G_0/G_1 cell cycle arrest in the stable cell lines. Taken together, these results indicated that 3D8 VL WT, but not NP25, reduced cell growth rate of the stable cell lines by inducing some levels of G_0/G_1 cell cycle arrest.

3.5. NP25 selectively hydrolyze mRNA levels of EGFP carrying the target sequence in the stable cell lines

We next evaluated whether ectopically expressed NP25 in the stable cell lines can selectively recognize to hydrolyze mRNA carrying the target sequence in the complicated cytosolic environment. For the reporter mRNA system, EGFP was employed by introducing the target asNP_{18} and off-target G_{18} sequence between ATG start codon and EGFP reading frame, generating asNP_{18}-EGFP and G_{18}-EGFP, respectively. The plasmid encoding intact EGFP, asNP_{18}-EGFP, or G_{18}-EGFP was transiently transfected into WT-1/-2 and NP25-1/-2 stable cell lines as well as mock cells. The cytosolic presence of WT and NP25 did not significantly hydrolyze the upcoming DNA during the transfection, as assessed by PCR of EGFP gene against the cellular DNA (Supplementary Fig. S5). The gene expression of EGFP was monitored at the mRNA level by semi-quantitative RT-PCR and at the protein level by Western blotting, confocal fluorescence microscopy, and flow cytometry. In mock cells, the mRNA and protein levels of EGFP were all comparable between the cells transfected with the plasmids of EGFP, asNP_{18}-EGFP, and G_{18}-EGFP (Fig. 3A–D), suggesting that the presence of N-terminal asNP_{18} or G_{18} sequence negligibly affects the expression of EGFP in the cells (Lee et al., 2010b). WT-1/-2 cells showed significant reduction in the mRNA and protein levels of EGFP and its fluorescence intensity regardless of the presence of the N-terminal target/off-target sequences, demonstrating the sequence non-specific hydrolyzing activity of 3D8 VL WT for the EGFP mRNAs leads to the gene-silencing in the cytosolic environment (Fig. 3A-D). In contrast, NP25-1/-2 cells selectively decreased the amount of asNP_{18}-EGFP at both mRNA and protein levels, without signifi-

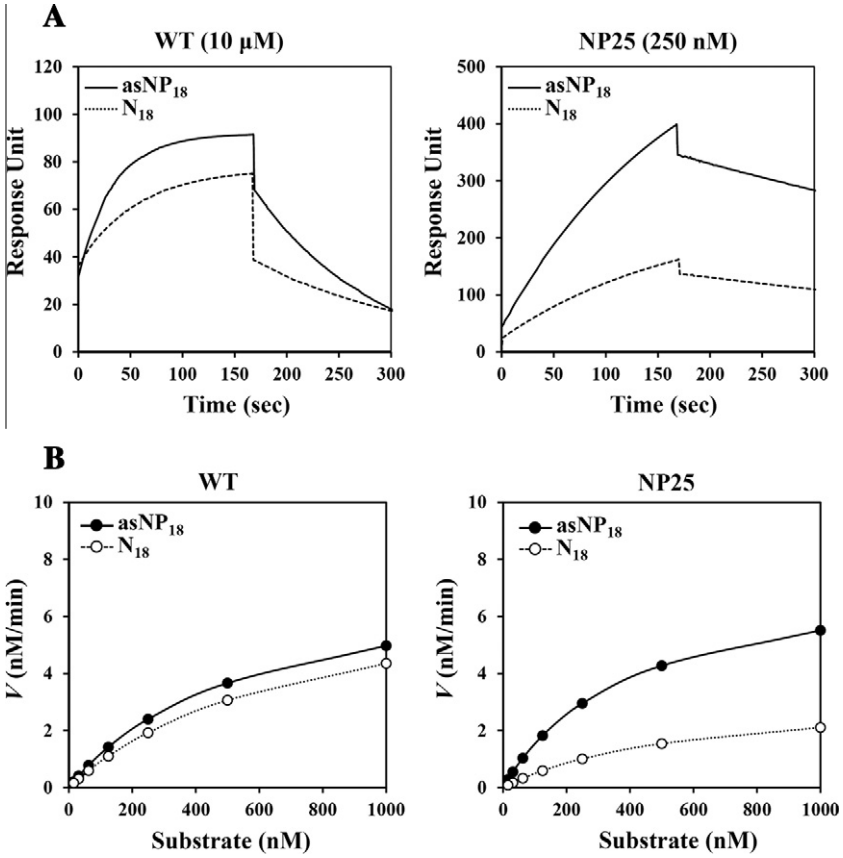

Fig. 1. The selected NP25 variant against $asNP_{18}$ substrate preferentially binds to hydrolyze the target substrates. (A) Representative SPR sensograms showing kinetic binding interactions between 3D8 VLs and 18-nt ssDNA substrates. SPR sensograms were obtained from injections of 3D8 VL WT (10 μM) or NP25 (0.25 μM) over $asNP_{18}$ or N_{18} substrate-immobilized surface at a flow rate of 30 μl/min. (B) Sequence-specific 18-nt ssDNA hydrolyzing assay of NP25 compared with 3D8 VL WT. Each protein (100 nM) was incubated at 37 °C with the indicated concentrations of $asNP_{18}$ or N_{18} substrate (16 nM–1 μM) and then the substrate-concentration dependent initial hydrolyzing velocity (V) of the protein was plotted against the substrate concentration. Lines through the mean values represent a mathematical fit of the data using the Michaelis–Menten equation. The detailed enzymatic kinetic parameters are shown in Table 2.

Table 1
Kinetic binding parameters for the interaction of 3D8 VLs with target $asNP_{18}$ and off-target N_{18} 18-nt ssDNAs, which were monitored by SPR.[a]

3D8 VLs	Kinetic parameters	18-nt ssDNAs	
		$asNP_{18}$	N_{18}
WT	k_{on} (M^{-1} s^{-1}) ($\times 10^3$)	1.76 ± 0.09	1.17 ± 0.09
	k_{off} (s^{-1}) ($\times 10^{-3}$)	9.14 ± 0.09	6.17 ± 0.11
	K_D (M) ($\times 10^{-7}$)	51.8 ± 0.6	52.9 ± 0.25
NP25	k_{on} (M^{-1} s^{-1}) ($\times 10^3$)	18.3 ± 0.2	3.78 ± 0.01
	k_{off} (s^{-1}) ($\times 10^{-3}$)	0.99 ± 0.01	3.11 ± 0.06
	K_D (M) ($\times 10^{-7}$)	0.54 ± 0.02	8.22 ± 0.15

[a] Each value represents the mean ± SD of two independent experiments. In each experiment, at least five sets were used in the determination of the kinetic constants.

cant effects on the mRNA and protein levels of intact EGFP, G_{18}-EGFP and house-keeping proteins (Fig. 3A and B). NP25 selectively abolished $asNP_{18}$-EGFP expression, but not EGFP and G_{18}-EGFP expression, as determined by confocal fluorescence microscopy (Fig. 3C) and flow cytometry (Fig. 3D). These results suggested that cytosolically expressed NP25 selectively degrades the mRNA carrying the target sequence of $asNP_{18}$, leading to the target gene-selective gene silencing, without significant effects on off-target RNAs.

3.6. NP25 inhibits H9N2 virus accumulation in the stable cell lines

To assess whether intracellular expression of $asNP_{18}$-selective NP25 is able to protect the stable A549 cell lines from the replication and production of H9N2 influenza virus carrying the target NP-vRNA genome, NP25-1/-2 cells as well as mock and WT-1/-2 cells as controls were infected with H9N2 virus at a m.o.i. of 0.0025, 0.01 and 0.04 and then culture supernatants were harvested at 24, 48, and 60 hpi to determine the virus titer by HA assay. In mock cells, virus titers dramatically increased over time in proportion to the challenged amount of virus (Fig. 4A). However, virus titers in the WT-1/-2 and NP25-1/-2 cell cultures were 2–50-folds lower depending on the virus infection m.o.i. and period than the mock cell cultures (Fig. 4A), demonstrating that virus replication had been effectively suppressed by the expression of 3D8 VL WT or NP25 in the cells. Although the expression levels of NP25 and 3D8 VL WT were similar in the stable cell lines, however, NP25-1/-2 cells showed 2- to 10-fold more reduction in the virus titers than with WT-1/-2 cells, suggesting that NP25 inhibits more potently the viral propagation than 3D8 VL WT in the cells. The representative raw data of HA assay are shown in Supplementary Fig. S6.

We also compared the protein levels of NP by Western blotting between the stable cell lines infected with H9N2 at a m.o.i. of 0.01 and 0.04 at 24 or 48 hpi. Compared with the mock cells, both NP25-1/-2 and WT-1/WT-2 cells displayed significant reduction in the amount of H9N2 NP protein (Fig. 4B). However, NP25-1/-2 cells showed more pronounced inhibitory effect on the NP protein levels than WT-1/-2 cells, particularly at the high m.o.i. of 0.04, consistent with the above virus titer results (Fig. 4A). Detection of H9N2 NP protein by confocal fluorescence microscopy conformed to the results of Western blotting (Fig. 4C).

Table 2
Kinetic parameters of 3D8 VLs hydrolyzing activity for target asNP$_{18}$ and off-target N$_{18}$ ss-DNA substrates, derived from the data given in Fig. 1B.[a]

3D8 VLs	Kinetic parameters	18-nt ssDNAs	
		asNP$_{18}$	N$_{18}$
WT	K_m (nM)	593.7 ± 14.7	728.9 ± 3.6
	k_{cat} (s^{-1}) ($\times 10^{-3}$)	2.1 ± 0.1	1.9 ± 0.1
	k_{cat}/K_m ($nM^{-1}\,s^{-1}$) ($\times 10^{-6}$)	3.5 ± 0.1	2.6 ± 0.1
NP25	K_m (nM)	407.8 ± 6.4	577.9 ± 24.3
	k_{cat} (s^{-1}) ($\times 10^{-3}$)	1.9 ± 0.1*	0.8 ± 0.1
	k_{cat}/K_m ($nM^{-1}\,s^{-1}$) ($\times 10^{-6}$)	4.8 ± 0.1*	1.4 ± 0.1

[a] All experiments were performed in triplicate and the results are represented as mean ± SD. Significant difference of each kinetic parameter was determined using a two-tailed Student's *t*-test versus the control N$_{18}$ substrate (*: $P < 0.01$).

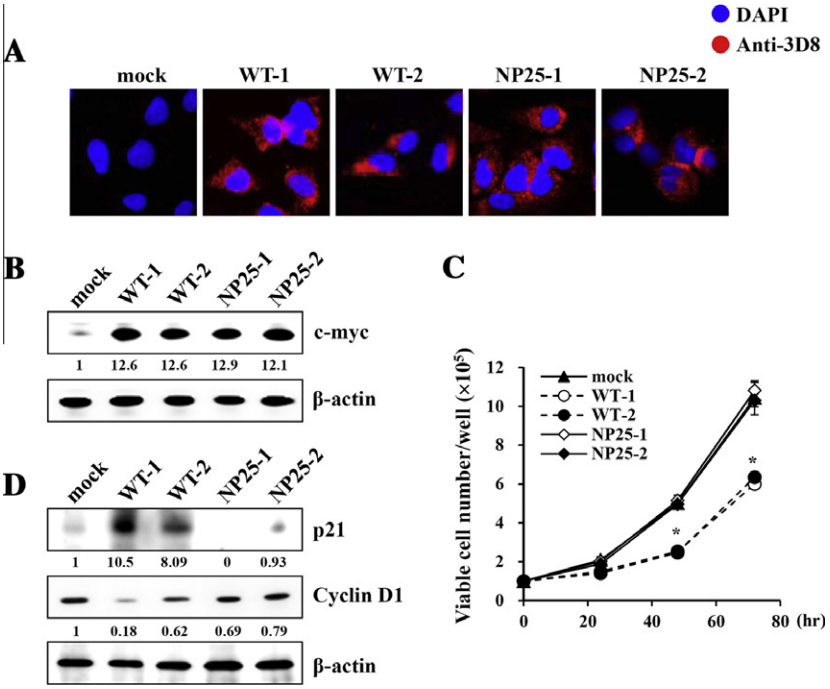

Fig. 2. Establishment of stable A549 cell lines constitutively expressing 3D8 VL WT or NP25 and their effects on the host cell growth rates. (A) Immunofluorescence detection of 3D8 VL proteins in the mock cells transfected with empty plasmid, WT-1/-2 cells expressing 3D8 VL WT, and NP25-1/-2 cells expressing NP25 by staining with rabbit polyclonal anti-3D8 antibodies followed by secondary TRITC-labeled anti-rabbit IgG. Images show the 3D8 VLs (red) and DAPI-stained nuclei (blue). Magnification, 400×. (B) Expression levels of 3D8 VL WT and NP25 in the established cell lines as in (A), determined by the C-terminal c-myc tag detection under Western blotting. (C) Viable cell number of the established A549 cell lines, which were seeded on 6-well plates (1×10^5/well) and further cultured for the indicated periods prior to the determination of cell number. Data represent mean ± SEM of the three independent experiments carried out in triplicate. *, $P < 0.01$ compared with the 'mock' cells. (D) The protein levels of p21^{Cip1} and cyclin D1 in the established cell lines, determined by Western blotting. In (B and D), the number below the panel indicates relative value of band intensity of proteins compared to the band intensity in 'mock' cells after normalization of the band intensity to that of β-actin for each sample. (For interpretation of the references to colour in this figure legend, the reader is referred to the web version of this article.)

To address the antiviral specificity of NP25 for H9N2 in NP25-1/-2 cells, the cells were infected with (−)-ssRNA-genomed vesicular stomatitis virus (VSV), which does not have the targeted NP-vRNA. VSV infection into NP25-1 cells exhibited comparable cytopathicity and viral titer to those in the mock cells (Supplementary Fig. S7), indicating that NP25 expression did not confer any antiviral activity on NP25-1 cells against VSV. However, WT-1/-2 cells were more resistant than NP25-1/-2 cells against VSV-induced cell death and the virus titer from WT-1 cells was significantly lower (~25%) than those from mock and NP25-1 cells, which can be attributed to the sequence-nonspecific hydrolyzing activity of viral RNAs, as observed in our previous study (Jun et al., 2010). These results suggested that antiviral activity of NP25-1/-2 cells against H9N2 virus is specifically mediated by NP25 expression in the cells.

3.7. NP25 preferentially decreases the amount of the targeted NP-vRNA in the stable cell lines

To evaluate whether NP25 inhibits the H9N2 virus propagation by degrading the NP-vRNA carrying the target sequence of asNP$_{18}$, we monitored the accumulation of NP-vRNA and off-target M2-vRNA in the NP25-1 cells, in comparison with WT-1 cells, after viral infection at a m.o.i. of 0.01 and 0.04. Further, we also monitored the levels of NP-mRNA and M2-mRNA under the same condition. Transcription of the (−)-stranded vRNA produces the complementary, (+)-stranded mRNA and thus the two RNAs can be independently converted to cDNA by using specific primers (Ge et al., 2003). After influenza virus infection, new virions are released in ~4 h (Medina and Garcia-Sastre, 2011; Scull and Rice, 2010). In

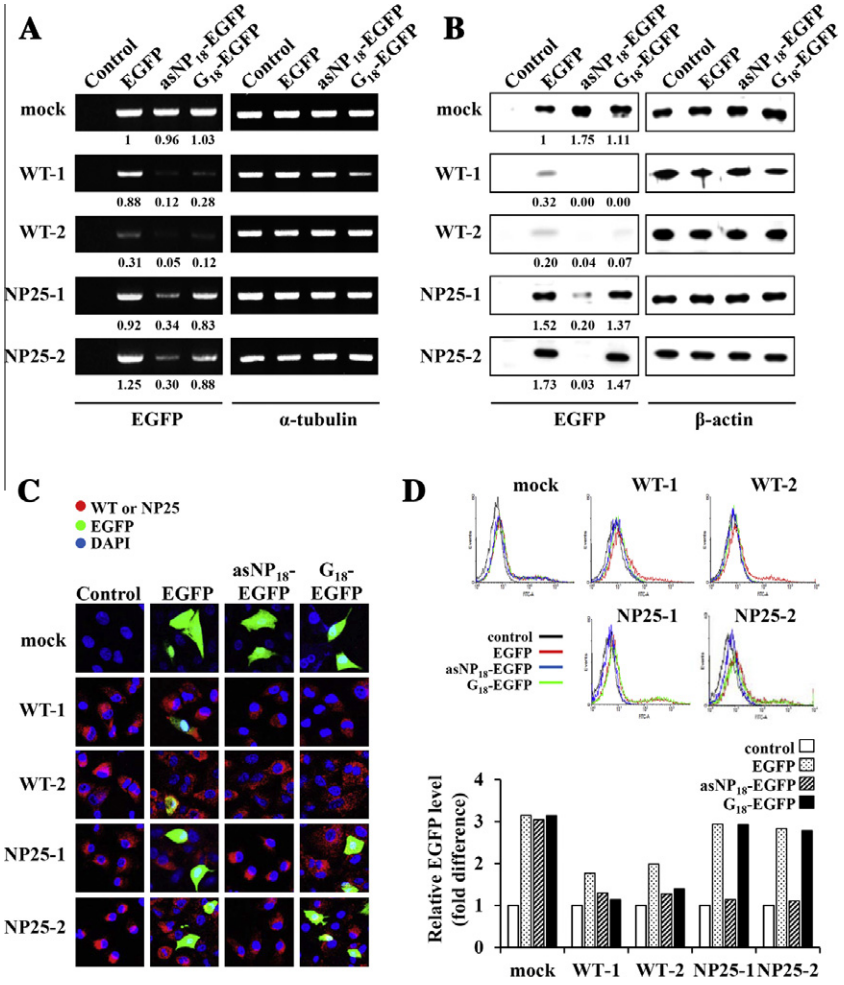

Fig. 3. NP25 selectively reduces the mRNA level of the EGFP reporter gene carrying the target sequence, leading to the target gene-silencing, in the stable A549 cell lines. The stable cell lines of NP25-1/-2 and WT-1/-2 cells and mock cells were untransfected ('Control') or transfected with plasmids encoding intact EGFP, asNP$_{18}$-EGFP, or G$_{18}$-EGFP for 4 h, further incubated for 24 h, and then monitored EGFP mRNA levels by RT-PCR (A) and EGFP protein levels by Western blotting (B), confocal fluorescence microscopy (C), and flow cytometry (D). Transfection efficiency of the plasmids was about 20% based on the EGFP expression. In (A and B), the number below the panel indicates relative band intensity of mRNA (A) or proteins (B) compared to the band intensity in the mock cells transfected with the plasmid encoding intact EGFP (pEGFP-N1) after normalization of the band intensity to that of α-tubulin (A) or β-actin (B) for each sample. In (C), fluorescence image of EGFP (green), nuclei (blue) stained with DAPI, and/or WT/NP25 (red) stained with rabbit anti-3D8 polyclonal antibodies and then TRITC-labeled anti-rabbit IgG were merged. Magnification, 200×. In (D), flow cytometry analysis of EGFP expression (upper panel) and the relative EGFP fluorescence levels (lower panel), which were calculated by comparing the mean fluorescence intensity with that of the control cells untransfected. Endogenous α-tubulin or β-actin served as the mRNA abundance and protein loading control for RT-PCR or Western blotting, respectively. (For interpretation of the references to colour in this figure legend, the reader is referred to the web version of this article.)

order to follow up abundance of viral RNAs in a cohort of synchronically infected cells (i.e., before new virion release and reinfection), total RNAs were isolated from the virus-infected cells at 1 and 3 hpi and assessed by RT and real-time PCR. In NP25-1 and WT-1 cells, the levels of vRNAs and mRNAs encoding NP and M2 genes were ~2–25-fold lower than those in the mock cells with more pronounced effects at the high dosage infection and the later hpi, suggesting that the antiviral activity of 3D8 VL WT and NP25 is mediated by decreasing viral vRNAs and/or mRNAs in the cells (Fig. 5A). Importantly, the levels of NP-vRNA in NP25-1 cells was ~2-fold and ~3-fold lower at 3 hpi after viral infection with m.o.i of 0.01 and 0.04, respectively, compared with those of NP-vRNA in WT-1 cells (Fig. 5A). However, M2-vRNA in NP25-1 cells showed more than 5-fold higher levels at 3 hpi after viral infection with m.o.i of 0.01 or 0.04, compared with NP-vRNA levels in NP25-1 cells. These results suggest that NP25 selectively degrades the targeted NP-vRNA over the off-target M2-vRNA. The similar results were also obtained when the levels of NP-vRNA and M2-vRNA were quantified at 3 hpi by semi-quantitative RT-PCR after the viral infection at a m.o.i. of 0.0025, 0.01 or 0.04 (Fig. 5B). Noticeably, the amount of NP-mRNA was also more selectively decreased in NP25-1 cells compared with M2-mRNA in NP25-1 cells and NP-mRNA in WT-1 cells (Fig. 5A and B). It seems that the preferential depletion of NP-vRNA by NP25 seems to contribute to more substantial reduction in the abundance of its transcript NP-mRNA than M2-mRNA. In WT-1 cells, the vRNA and mRNA levels of NP and M2 gene were all decreased at the similar levels, compared with the mock cells (Fig. 5B). There were no significant changes in the mRNA levels of endogenous α-tubulin mRNA in the early period of 3 hpi (Fig. 5B), suggesting that viral RNAs are more susceptible to degradation than cellular RNAs by NP25 and 3D8 VL WT in the stable cell lines. Taken together, these results suggested that NP25 selectively recognizes to degrade the targeted NP-vRNA from the first viral infection stage, leading to potent inhibition of the viral replication and new virion production in the stable cell lines.

4. Discussion

In this study we have shown a novel approach of targeting particular viral genomic RNAs for degradation by antibody with the sequence-specific nucleic acid hydrolyzing activity for the inhibi-

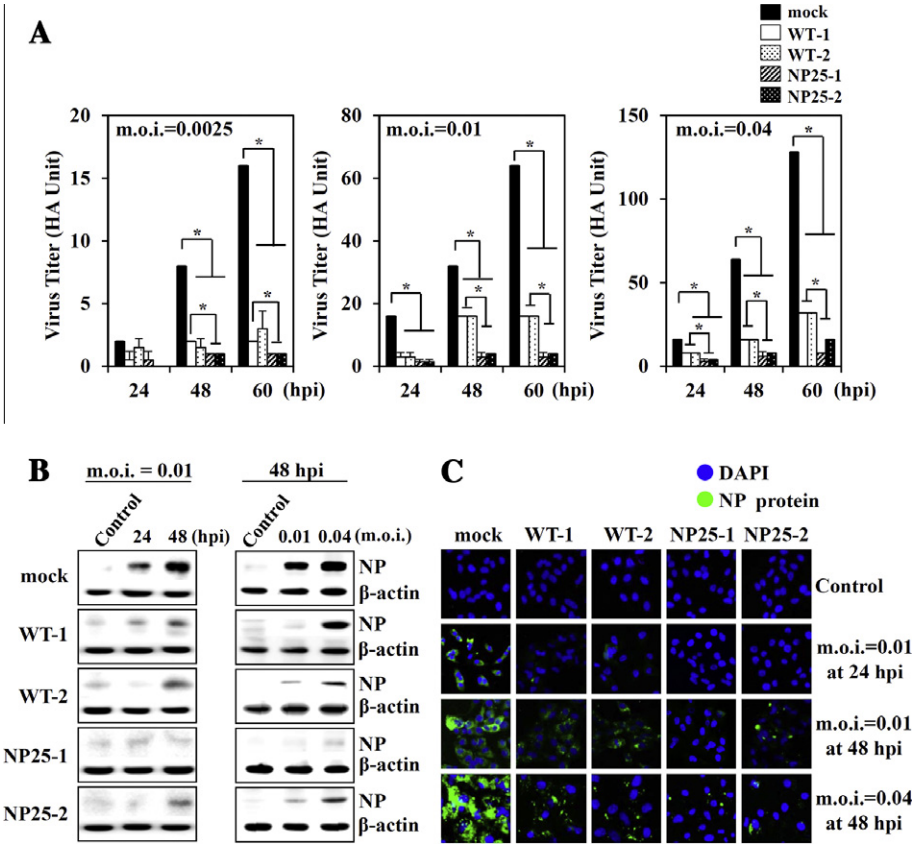

Fig. 4. NP25 more potently inhibits the replication of H9N2 influenza virus than 3D8 VL WT in the stable A549 cell lines. (A) Inhibition of H9N2 virus production in the stable cell lines. Each cell line was infected with H9N2 virus at a m.o.i. of 0.0025, 0.01 or 0.04, and then further incubated for 24, 48, and 60 h prior to the determination of viral titers in the culture supernatants by HA assay. Data represent mean ± SEM of two independent experiments carried out in triplicate. *, $P < 0.05$ compared with the mock or WT-1/-2 cells as indicated. (B and C) Downregulation of NP at the protein levels in the stable cell lines, monitored by Western blotting (B) and confocal fluorescence microscopy (C). Each cell line was infected with H9N2 virus at a m.o.i. of 0.01 or 0.04, and then further incubated for 24 or 48 h prior to the analyses. In (B and C), 'Control' designates uninfected cells. In (C), green color represents viral NP protein, while blue color represents DAPI-stained nuclei. Magnification, 100×. (For interpretation of the references to colour in this figure legend, the reader is referred to the web version of this article.)

tion of viral propagation. We isolated NP25 which preferentially binds to hydrolyze the 18-nt substrate with asNP$_{18}$ sequence derived from NP-vRNA of H9N2 influenza virus. The cytosolic expression of asNP$_{18}$-selective NP25 in the stable A549 cell lines does not show significant cytotoxicity, which is mediated by the sequence-nonspecific nucleic acid hydrolyzing 3D8 VL WT, and significantly protects the stable cell lines from H9N2 virus replication by selective degradation of the target NP-vRNA. This is the first study describing the engineered catalytic antibody-based antiviral strategy of targeting viral genome itself rather than their gene products or mRNA itself.

Some RNases have been shown to suppress viral replication in animal cells. Overexpression of ISG20, a human RNase specific for ssRNA, in HeLa cells showed resistance to infections by various viruses with ssRNA genomes, such as vesicular stomatitis and influenza viruses, but not to the DNA genomic adenovirus (Espert et al., 2003). An amphibian RNase, Onconase, inhibited the replication of human immunodeficiency virus, type I (HIV-1), which has (−)-ssRNA as a genome in a chronically HIV-1-infected human cells (Saxena et al., 1996). In this study we have shown that the cytosolic expression of 3D8 VL WT efficiently suppressed the replication of H9N2 virus with (−)-ssRNA genome, like the 3D8 scFv that exhibited an antiviral activity against classical swine fever virus with (+)-ssRNA genome (Jun et al., 2010). Despite of the sequence-nonspecific RNA hydrolyzing activity, 3D8 VL WT more selectively hydrolyzed viral RNAs than the endogenous cellular RNAs (Figs. 4 and 5), like the antiviral RNases and 3D8 scFv (Jang et al., 2009; Saxena et al., 2002). It seems that endogenous cellular RNAs associated with cellular proteins are more efficiently protected than viral RNAs from the RNA hydrolyzing activity of 3D8 VL WT (Figs. 3–5). Thus the preferential degradation of viral RNAs over cellular RNAs by 3D8 VL WT might explain the antiviral activity, as proposed for the antiviral mechanism of Onconase and 3D8 scFv with no sequence specificity (Jang et al., 2009; Jun et al., 2010; Saxena et al., 1996, 2002).

However, 3D8 VL WT without the particular specificity for RNA sequence and/or structure shows some levels of cytotoxicity by inducing cell cycle arrest to slow the cell proliferation rate even in the established A549 stable cell lines (Fig. 2). This result is consistent with previous observations that microinjected Onconase or RNase A induced cell death by cell cycle arrest (Smith et al., 1999). Thus the cytotoxicity of 3D8 VL WT most likely resulted from the nonspecific hydrolysis of cellular RNAs, like the cases of Onconase and 3D8 scFv (Jang et al., 2009; Saxena et al., 2009; Smith et al., 1999). In contrast to 3D8 VL WT, NP25 with ~15-fold higher affinity and ~3-fold greater selective hydrolyzing activity for the target asNP$_{18}$ substrate than for off-target N$_{18}$ substrate does not show any significant cytotoxicity to the host cells. Further, NP25 selectively induces knockdown of the reporter EGFP carrying the target sequence at 5′-terminus by decreasing the mRNA level with minimal effects on off-target mRNAs in the cytosolic environment (Fig. 3). Thus the conferred target specificity of NP25 overcome the undesirable cytotoxicity mediated by its parent 3D8 VL WT.

The cytosolic expression of asNP$_{18}$-selective NP25 more efficiently inhibited the accumulation of H9N2 virus (A/Chicken/Korea/MS96/96) than 3D8 VL WT in the stable cell lines. More

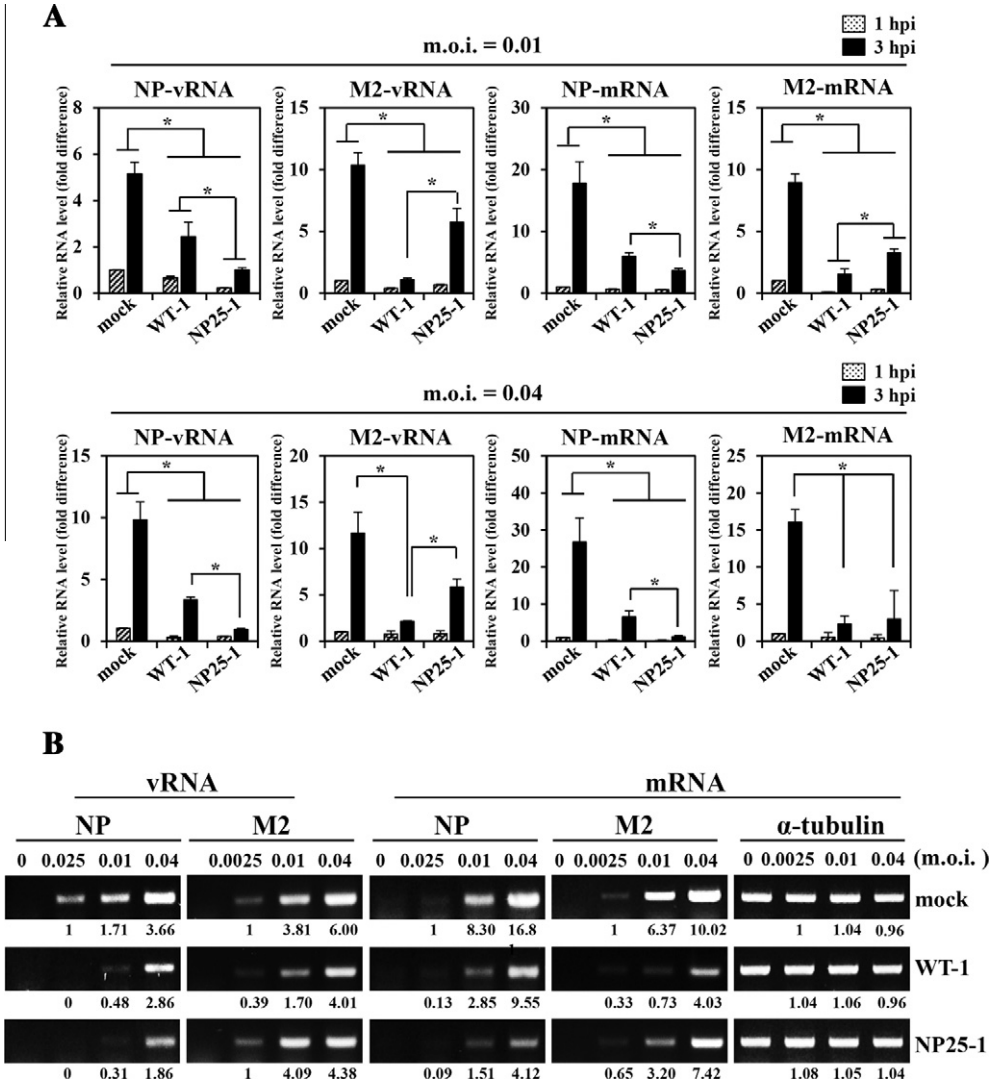

Fig. 5. NP25 more selectively decreases the amount of the targeted NP-vRNA than 3D8 VL WT in the stable A549 cell lines in the early infection periods. (A and B) The levels of NP-vRNA, NP-mRNA, M2-vRNA, and M2-mRNA of H9N2 virus in the virus-infected stable cell lines, monitored by RT, followed by real-time PCR at 1 and 3 hpi (A) and semi-quantitative PCR at 3 hpi (B) using each RNA gene specific primers. Cells were infected with H9N2 virus at a m.o.i. of 0.0025, 0.01 and/or 0.04 and then harvested for RNA extraction at 1 and/or 3 hpi. In (A), the level of each viral RNA was normalized to the level of α-tubulin mRNA of the host cells and then presented as fold difference compared to those in the mock cells at 1 hpi. Data represent mean ± SEM of two independent experiments carried out in triplicate. *, $P < 0.05$ compared with the mock or WT-1/-2 cells as indicated. In (B), the level of endogenous α-tubulin mRNA was included as an mRNA abundance control. The number below the panel indicates relative value of band intensity compared to the value of 'mock' cells infected at a m.o.i. 0.0025.

specific reduction in the amount of targeted NP-vRNA than off-target M2-vRNA from the early stage of virus infection in the stable cell lines without noticeable changes in the levels of the endogenous mRNA suggests that NP25 indeed recognizes and hydrolyzes the NP-vRNA of H9N2 virus more specifically than off-targets. The preferential degradation of NP-vRNA by NP25 seems to cause more significant reduction in the amount of NP-mRNA, the transcript of NP-vRNA, compared with M2-mRNA. In addition to the targeted NP-vRNA, the off-targets of NP-mRNA, M2-vRNA and M2-mRNA were also decreased in NP25-1 cells. NP is critical for replication of vRNAs (Kao et al., 2010; Muller et al., 2012). Accordingly, depletion of NP-vRNA by NP25 seems to exert a global effect, inhibiting the accumulation of other viral RNAs, including M2-vRNA (Ge et al., 2003). However, NP25 did not inhibit the accumulation of M2-vRNA as much as NP-vRNA (Fig. 5). This can be attributed to the difference in the timing of mRNA transcription and cRNA/vRNA replication. After influenza virus infection, mRNA production and protein synthesis precede genome replication (Muller et al., 2012; Scull and Rice, 2010). Immediately synthesized NP protein upon H9N2 virus infection (before NP-vRNA degradation by NP25) may contribute to some levels of the off-target M2-vRNA in NP25-1 cells.

After internalization of influenza A virus into cells, the genomic vRNAs enter into the nucleus of cells and serves as templates for the transcription of viral mRNAs and cRNAs (Medina and Garcia-Sastre, 2011; Subbarao and Joseph, 2007). Accumulation of viral proteins switches on the replication of vRNAs based on the template of (+)-cRNAs in the nucleus (Muller et al., 2012; Scull and Rice, 2010). Naked vRNAs route to cytosol and then are encapsidated by NP before the assembly with other viral proteins and release from the host. Considering the life cycle of influenza A virus, cytosolically expressed NP25 has a chance to recognize naked NP-vRNA only in the cytosol before its assembly with viral proteins. NP25 did not completely abolish but reduce the accumulation of NP-vRNA, particularly at high-titer infection of virus. Thus further engineering of NP25 to have much higher specific hydrolyzing

activity for the target NP-vRNA seems to be necessary for the complete inhibition of virus replication. In another aspect, if NP25 is directed to be localized in the nucleus of cells, where vRNAs are amplified, it might more effectively inhibit the viral replication.

5. Conclusions

Influenza NP is essential to viral replication, providing an ideal target for antiviral therapy (Medina and Garcia-Sastre, 2011). NP has been targeted at the protein level for antiviral therapy by a small molecule (Kao et al., 2010), but it is extremely difficult to be targeted by antibody since it is not exposed at the viral surface. Thus NP gene has been targeted at the mRNA level using siRNA technique, showing effective inhibition of influenza A virus replication in the cells expressing the siRNA (Ge et al., 2003; Zhou et al., 2007, 2008). However, antiviral therapy by siRNA has a disadvantage over protein-based approach, such as antibody, because siRNA is much less stable than proteins due to the susceptibility to RNases (Manikandan et al., 2007). In this study NP gene is targeted at the viral genomic vRNA level by single domain antibody, NP25, which can selectively recognize and hydrolyze the targeted NP-vRNA from the initial infection stage. The asNP_{18} target sequences of NP-vRNA in the low pathogenic H9N2 are highly conserved in other NP-vRNAs of high pathogenic viruses, such as H1N1 (A/PuertoRico/8/34) and H5N1 (A/chicken/Hubei/327/2004). Therefore, NP25 against NP-vRNA might have a potential capability of broad inhibition of the high pathogenic influenza A viruses. Our results provide a proof-of-concept of targeting viral genomic vRNAs by the sequence-specific nucleic acid hydrolyzing antibody for the prevention and control of influenza A virus infection in humans and animals.

Acknowledgements

This work was supported by Mid-career Researcher Program (2010-0009760) and Priority Research Centers Program (2011-0022978) through the National Research Foundation of Korea (NRF) of the MEST and by the Biogreen 21 program (PJ007068) of Rural Development Administration, Republic of Korea.

Appendix A. Supplementary data

Supplementary data associated with this article can be found, in the online version, at http://dx.doi.org/10.1016/j.antiviral.2012.03.007.

References

Barik, S., 2010. SiRNA for influenza therapy. Viruses 2, 1448–1457.
Choi, Y.K., Seo, S.H., Kim, J.A., Webby, R.J., Webster, R.G., 2005. Avian influenza viruses in Korean live poultry markets and their pathogenic potential. Virology 332, 529–537.
Daelemans, D., Pauwels, R., De Clercq, E., Pannecouque, C., 2011. A time-of-drug addition approach to target identification of antiviral compounds. Nat. Protoc. 6, 925–933.
Espert, L., Degols, G., Gongora, C., Blondel, D., Williams, B.R., Silverman, R.H., Mechti, N., 2003. ISG20, a new interferon-induced RNase specific for single-stranded RNA, defines an alternative antiviral pathway against RNA genomic viruses. J. Biol. Chem. 278, 16151–16158.
Ge, Q., McManus, M.T., Nguyen, T., Shen, C.H., Sharp, P.A., Eisen, H.N., Chen, J., 2003. RNA interference of influenza virus production by directly targeting mRNA for degradation and indirectly inhibiting all viral RNA transcription. Proc. Natl. Acad. Sci. USA 100, 2718–2723.
Jang, J.Y., Jeong, J.G., Jun, H.R., Lee, S.C., Kim, J.S., Kim, Y.S., Kwon, M.H., 2009. A nucleic acid-hydrolyzing antibody penetrates into cells via caveolae-mediated endocytosis, localizes in the cytosol and exhibits cytotoxicity. Cell. Mol. Life Sci. 66, 1985–1997.
Jun, H.R., Pham, C.D., Lim, S.I., Lee, S.C., Kim, Y.S., Park, S., Kwon, M.H., 2010. An RNA-hydrolyzing recombinant antibody exhibits an antiviral activity against classical swine fever virus. Biochem. Biophys. Res. Commun. 395, 484–489.
Kao, R.Y., Yang, D., Lau, L.S., Tsui, W.H., Hu, L., Dai, J., Chan, M.P., Chan, C.M., Wang, P., Zheng, B.J., Sun, J., Huang, J.D., Madar, J., Chen, G., Chen, H., Guan, Y., Yuen, K.Y., 2010. Identification of influenza A nucleoprotein as an antiviral target. Nat. Biotechnol. 28, 600–605.
Kim, Y.R., Kim, J.S., Lee, S.H., Lee, W.R., Sohn, J.N., Chung, Y.C., Shim, H.K., Lee, S.C., Kwon, M.H., Kim, Y.S., 2006. Heavy and light chain variable single domains of an anti-DNA binding antibody hydrolyze both double- and single-stranded DNAs without sequence specificity. J. Biol. Chem. 281, 15287–15295.
Kim, D.S., Lee, S.H., Kim, J.S., Lee, S.C., Kwon, M.H., Kim, Y.S., 2009. Generation of humanized anti-DNA hydrolyzing catalytic antibodies by complementarity determining region grafting. Biochem. Biophys. Res. Commun. 379, 314–318.
Kwon, H.J., Kim, H.H., Yoon, S.Y., Ryu, Y.B., Chang, J.S., Cho, K.O., Rho, M.C., Park, S.J., Lee, W.S., 2010. In vitro inhibitory activity of *Alpinia katsumadai* extracts against influenza virus infection and hemagglutination. Virol. J. 7, 307.
Lee, C.H., Park, K.J., Sung, E.S., Kim, A., Choi, J.D., Kim, J.S., Kim, S.H., Kwon, M.H., Kim, Y.S., 2010a. Engineering of a human kringle domain into agonistic and antagonistic binding proteins functioning in vitro and in vivo. Proc. Natl. Acad. Sci. USA 107, 9567–9571.
Lee, W.R., Jang, J.Y., Kim, J.S., Kwon, M.H., Kim, Y.S., 2010b. Gene silencing by cell-penetrating, sequence-selective and nucleic-acid hydrolyzing antibodies. Nucleic Acids Res. 38, 1596–1609.
Manikandan, J., Pushparaj, P.N., Melendez, A.J., 2007. Protein i: interference at protein level by intrabodies. Front. Biosci. 12, 1344–1352.
Medina, R.A., Garcia-Sastre, A., 2011. Influenza A viruses: new research developments. Nat. Rev. Microbiol. 9, 590–603.
Muller, K.H., Kakkola, L., Nagaraj, A.S., Cheltsov, A.V., Anastasina, M., Kainov, D.E., 2012. Emerging cellular targets for influenza antiviral agents. Trends Pharmacol. Sci. 33, 89–99.
Park, S.Y., Lee, W.R., Lee, S.C., Kwon, M.H., Kim, Y.S., Kim, J.S., 2008. Crystal structure of single-domain VL of an anti-DNA binding antibody 3D8 scFv and its active site revealed by complex structures of a small molecule and metals. Proteins 71, 2091–2096.
Saxena, S.K., Gravell, M., Wu, Y.N., Mikulski, S.M., Shogen, K., Ardelt, W., Youle, R.J., 1996. Inhibition of HIV-1 production and selective degradation of viral RNA by an amphibian ribonuclease. J. Biol. Chem. 271, 20783–20788.
Saxena, S.K., Sirdeshmukh, R., Ardelt, W., Mikulski, S.M., Shogen, K., Youle, R.J., 2002. Entry into cells and selective degradation of tRNAs by a cytotoxic member of the RNase A family. J. Biol. Chem. 277, 15142–15146.
Saxena, A., Saxena, S.K., Shogen, K., 2009. Effect of Onconase on double-stranded RNA in vitro. Anticancer Res. 29, 1067–1071.
Scull, M.A., Rice, C.M., 2010. A big role for small RNAs in influenza virus replication. Proc. Natl. Acad. Sci. USA 107, 11153–11154.
Sherr, C.J., Roberts, J.M., 1995. Inhibitors of mammalian G1 cyclin-dependent kinases. Genes Dev. 9, 1149–1163.
Smith, M.R., Newton, D.L., Mikulski, S.M., Rybak, S.M., 1999. Cell cycle-related differences in susceptibility of NIH/3T3 cells to ribonucleases. Exp. Cell Res. 247, 220–232.
Subbarao, K., Joseph, T., 2007. Scientific barriers to developing vaccines against avian influenza viruses. Nat. Rev. Immunol. 7, 267–278.
Sui, H.Y., Zhao, G.Y., Huang, J.D., Jin, D.Y., Yuen, K.Y., Zheng, B.J., 2009. Small interfering RNA targeting m2 gene induces effective and long term inhibition of influenza A virus replication. PLoS ONE 4, e5671.
Sung, E.S., Kim, A., Park, J.S., Chung, J., Kwon, M.H., Kim, Y.S., 2010. Histone deacetylase inhibitors synergistically potentiate death receptor 4-mediated apoptotic cell death of human T-cell acute lymphoblastic leukemia cells. Apoptosis 15, 1256–1269.
Wan, H., Sorrell, E.M., Song, H., Hossain, M.J., Ramirez-Nieto, G., Monne, I., Stevens, J., Cattoli, G., Capua, I., Chen, L.M., Donis, R.O., Busch, J., Paulson, J.C., Brockwell, C., Webby, R., Blanco, J., Al-Natour, M.Q., Perez, D.R., 2008. Replication and transmission of H9N2 influenza viruses in ferrets: evaluation of pandemic potential. PLoS ONE 3, e2923.
Zhou, H., Jin, M., Yu, Z., Xu, X., Peng, Y., Wu, H., Liu, J., Liu, H., Cao, S., Chen, H., 2007. Effective small interfering RNAs targeting matrix and nucleocapsid protein gene inhibit influenza A virus replication in cells and mice. Antiviral Res. 76, 186–193.
Zhou, K., He, H., Wu, Y., Duan, M., 2008. RNA interference of avian influenza virus H5N1 by inhibiting viral mRNA with siRNA expression plasmids. J. Biotechnol. 135, 140–144.